Environment, Development and Sustainability
https://doi.org/10.1007/s10668-020-01144-8

Subsurface nutrient modelling using finite element model under Boro rice cropping system

Ayushi Gupta[1] · Manika Gupta[2] · Prashant K. Srivastava[1,3] · Avijit Sen[4] · Ram Kumar Singh[4]

Received: 5 September 2020 / Accepted: 3 December 2020

Abstract

Boro rice, an emerging low-risk crop variety of rice, cultivated using residual or stored water after *Kharif* season. To enhance the quality and production of rice, potassium (K) and phosphorus (P) are the common constituents of agricultural fertilizers. However, excess application of fertilizers causes leaching of nutrients and contaminates the groundwater system. Therefore, assessment and optimization of fertilizer dose are needed for better management of fertilizers. Towards this, the present study determines the path, persistence, and mobility of K and P under the Boro rice cropping system. The experimental site consisted of four plots having Boro rice with four different fertilizer doses of nitrogen (N), P, K viz. 100%, 75%, 50%, and 25% of the recommended dose. Disturbed soil samples were analysed for K and P from pre-sown land to tillering stage at 0–5, 5–10, 10–15, 15–30, 30–45, and 45–60 cm depths. Simultaneously, K and available P were also simulated in the subsurface soil layers through the HYDRUS-1D model. The statistical comparisons were made with RMSER, E, and PBIAS between the modelled values and laboratory-measured values. Although, the results showed that all the treatments considered had agreeable simulations for both K and P, the K simulations were found to be better as compared to P simulations except for 25% where P simulations outperformed K. The simulated concentration at all doses was found most appropriate when measured for the subsurface layers (up to 45 cm), while showed an underestimation in the bottom layers (45–60 cm) of soil.

Keywords HYDRUS-1D · Boro rice · Subsurface modelling · Optimization

✉ Prashant K. Srivastava
prashant.iesd@bhu.ac.in; prashant.just@gmail.com

[1] Remote Sensing Laboratory, Institute of Environment and Sustainable Development, Banaras Hindu University, Varanasi, India

[2] Department of Geology, University of Delhi, New Delhi, India

[3] DST-Mahamana Centre of Excellence in Climate Change Research, Institute of Environment and Sustainable Development, Banaras Hindu University, Varanasi, India

[4] Department of Agronomy, Institute of Agricultural Sciences, Banaras Hindu University, Varanasi, India

Published online: 23 January 2021

1 Introduction

India has one of the world's largest land areas (44 million ha) under rice cultivation providing a 21% contribution to global rice production accounting for 148.3 million tonnes of rice production making it the second largest producer of rice in the world (CO et al. 2011 In Asia, more than two billion people are getting 60–70% of their energy requirement from rice and its derived products (FAOSTAT Database 2014). According to the FAO 2005 report, paddy alone consumes 31.8% of the total country's fertilizer ingested into the soil. Rice cultivation consumes a significant amount of fertilizer in India which has made paddy fields a large contributor to non-point source pollution. The understanding of nutrient/fertilizer transformation and transport in the case of paddy fields is very limited due to multipart interactions between the soil, water, and biomass (De Datta 1986). Our understanding of the production factors and constraints, which tend to reduce yield and productivity in rice farming, are still very limited to help formulate proper strategies to tackle them (Sarangi et al. 2014).

The word "Boro" is a special type of rice cultivated in the *Rabi* season. Since there is a continuous increase in irrigation facilities and less dependence on rain in agriculture, the production of these rice varieties has amplified over the past few decades. In addition, farmers favour growing rice in the dry season as it offers lower risks and higher productivity in Boro rice in *Rabi* season than *Kharif* rice. Therefore, Boro rice offers a great way to boost and alleviate rice production in the eastern Indian states of Assam, Bihar, Odisha, Uttar Pradesh, and West Bengal (Singh 2003). Hence, Boro rice is now being cultivated outside the areas of its traditional boundaries leading to the emergence of a new cropping system which is now increased from 1.35 million hectares in 1991 to 2.95 million hectares in 2000 (Lal et al. 2013).

The expansion of Boro rice cultivation outside the traditional boundaries requires an increase in intensive use of agrochemicals as Indian soils are low to medium in macronutrients (FAO 2005). In continuous cropping, the addition of prejudicial and unmanaged nutrient (nitrogen or phosphorus alone) supply in form of chemical fertilizers without organic manure has resulted in a reduction in crop productivity and soil fertility (Masto 2004). K and available P are nutrients that often limit agricultural production in tropical soils hence they are principal constituents in many fertilizer formulations (Moterle et al. 2016). Agricultural practices have to be created to monitor the quantity of fertilizer still present at various soil depths so that its effects can be examined on groundwater and an assessment can be made for the consecutive fertilizer input for the next crop period to combat overdosing of fertilizers in agricultural fields. For doing so, forecasting subsurface pathways of water and pollutants (nutrient and pesticides) in paddy cultivation becomes crucial to control non-point sources of pollution. Sub-surface modelling is an effective, less time-consuming way to avoid tedious and expensive methods of assessment and reassessment of nutrients that are present in soil from agricultural or other practices with minimal input data. It is reported that models are well-versed in prediction and simulation for agricultural management and interactions that cannot be measured physically. Moreover, studies on P and K simulations are not very well-documented in the Indian marginal farming system.

The finite element model determining the persistence of pesticides has already been found successful hence widening our understanding regarding these models to determine the overdosing of the macronutrient would be the next logical step in the process (Gupta et al. 2014a). The present study undertaken determines the persistence and mobility of K and available P under real hydro-meteorological and cropping field conditions using

HYDRUS 1D. The outcome of this study would improve our understanding of the behaviour of P and K under real field conditions in the case of directly seeded rice (DSR).

2 Materials and methodology

2.1 Site selection

The agricultural farm site of BHU is one of the government-sponsored site having sophisticated sensors for hydro-meteorological measurements, temperature, soil moisture etc. All the four plots selected were hydraulically separated from each other by impermeable barriers of the wall of thickness 12 cm up to depth of 170 cm, which prevents subsurface water flow and intermixing of treatments across plots. The plots are also equipped with flow meters, a controlled irrigation system, etc. Hence, the site is ideal for subsurface modelling because of systematic arrangement and availability of equipment, data, etc. The 04 identical experimental plots were used, each plot measures 4 m long and 4 m wide in area. The layout of the field is provided in Fig. 1. The field experiment plots were randomly selected out of all plots present at the site. The climate of the U.P. (East) is primarily defined as humid subtropical with dry winter.

2.2 Methodology

The flowchart for the complete methodology is provided in Fig. 2. The details of the same are presented in this section and Sect. 3. The field preparation started on February 22, 2018. The Boro rice variety used was *Malviya Hu105.* The first split of NPK fertilizer was added after manual ploughing and levelling off the field followed by rice seed line sowing. The line-to-line distance was kept at 20 cm apart while the plant to plant was kept 2 cm apart in the same line. The dry rice seed was sowed in these beds. The water was sprinkled to moisten the field enough for initial growth. Further, the irrigation of the crop

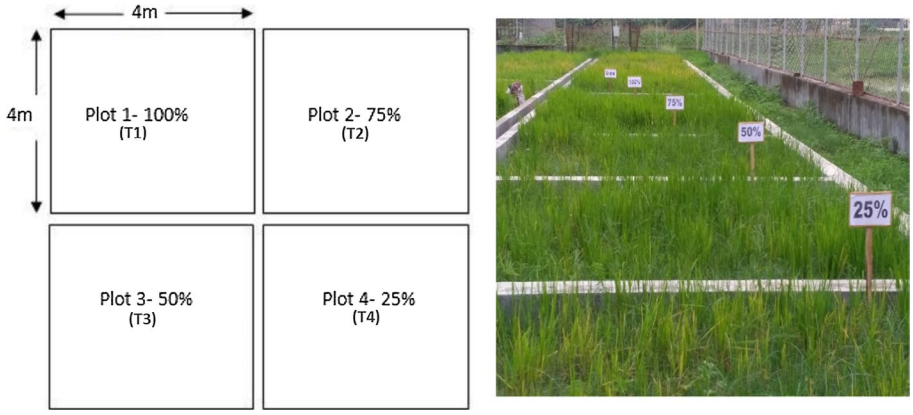

Fig. 1 Layout of fertilizer treatment design (left) and on field plantation image at 34 days after sowing (right) (note: percentage in figure represents the percent amount of recommended fertilizer dose added in the plots)

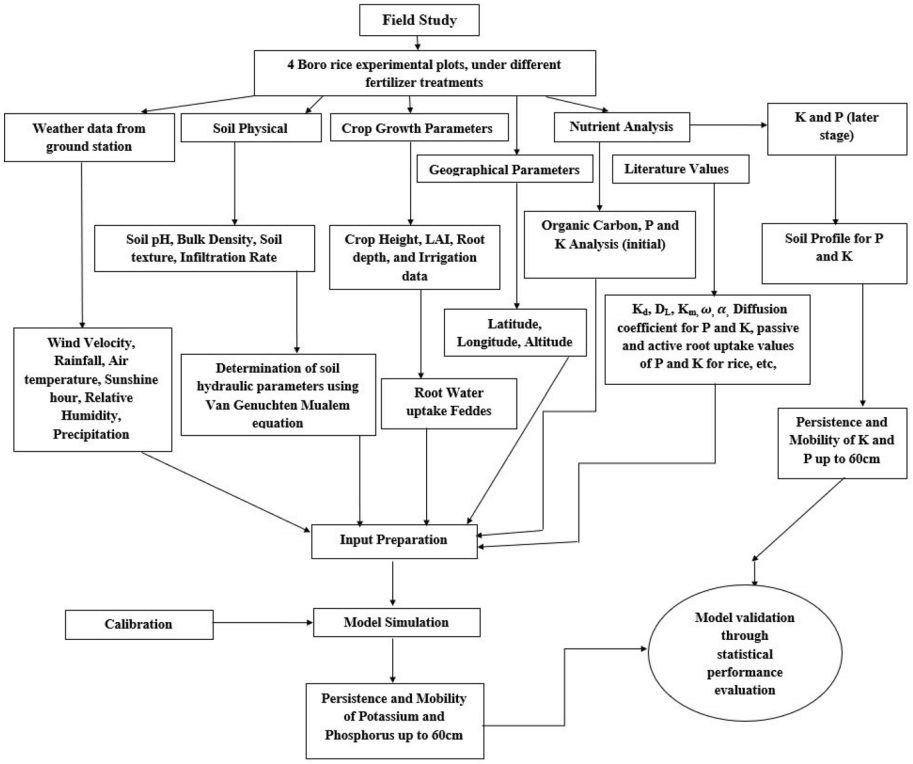

Fig. 2 Flowchart of the utilized methodology

was not fixed but was accounted for at each event. It changed according to the stages and seasonal variation to meet the real condition requirements. Hand weeding was done every 15–20 days. The fertilizer splits were added according to the treatment design as described in Sect. 2.3. All the reagents used for various tests were of analytical grade. A Hitachi UV–visible spectrophotometer model, U-1500, with 1 cm quartz cells cuvette was used for determination of P residue in the soil while Flame Photometer was used for K analysis.

2.3 Treatment design and soil analysis

The treatment scheme of fertilizer with its source is given in Table 1 with details of fertilizer application in Table 2. The diammonium phosphate and muriate of potash were added as a source for P and K, respectively, which were locally obtained as used by the farmers. The recommended dose prescribed by IRRI is 50 kg ha^{-1} for K and 65 kg ha^{-1} for P for rice in India. So, the treatments involved T1—100%, T2—75%, T3—50%, and T4—25% of the recommended dose for both K and P. K and P were applied only during the first split of fertilizer application.

The soil sampling was carried out in each of the four plots at four growth stages as mentioned in Table 3 for the soil profile at the depths: 0–5 cm, 5–10 cm, 10–15 cm, 15–30 cm, 30–45 cm and 45–60 cm. The two soil samples collected from the same plot at each layer were used to create a composite sample. The samples were stored in Ziploc soon

Table 1 Fertilizer treatment variations with their respective source

Treatment	Name	Treatment details
(Plot-1)	T1 100% recommended optimum dose of fertilizer NPK	[Urea (N): diammonium phosphate (P): muriate of potash (K)]
(Plot-2)	T2 75% recommended optimum dose of fertilizer NPK	[Urea (N): diammonium phosphate (P): muriate of potash (K)]
(Plot-3)	T3 50% recommended optimum dose of fertilizer NPK	[Urea (N): diammonium phosphate (P): muriate of potash (K)]
(Plot-4)	T4 25% recommended optimum dose of fertilizer NPK	[Urea (N): diammonium phosphate (P): muriate of potash (K)]

Table 2 Details of fertilizer split and application dates during trial

Season	Date	Agricultural activities
Rabi	26.02.18	Rice sowing (seed rate = 130 kg/ha), First split fertilizer application NPK (160:65:60)
	22.04.18	Second split fertilizer application N
	11.05.18	Third split fertilizer application N
	01.10.18	Field dried (drainage period)
	09.10.18	Harvesting

Table 3 Tabular representation of sampling days corresponding to plant's growing stage

SI no.	Date	Days after application (DAA)	Stage of crop
1	22 February 2018	0	Bare land
2	30 March 2018	34	Germination
3	23 May 2018	86	Seedling emergence
4	02 August 2018	158	Late vegetative

DAA days after application

after extraction from the plots. The initial concentration of available P and K in the soil was determined before the application of the fertilizer for all four plots. The samples were immediately stored under refrigeration conditions until analysis. The refrigerated soil samples were oven-dried, grounded, and sieved before available P was experimentally measured using the Olsen method (INTER 2011) and K was analyzed using Flame Photometer (Pawar et al. 2009). A total number of 120 samples were collected from the four plots during the experiment. The field plot is supported with daily ground-based measured data for daily metrological data like precipitation, sunshine hour, mean temperature, wind speed, etc. These data were recorded during the whole crop trial each day.

3 Numerical simulations

The transport of available P and K in the case of Boro rice was numerically simulated using Hydrus-1D (Šimunek and van Genuchten 2008). The detailed setup of Hydrus-1D and its parameterizations are provided in the following sections.

3.1 Time information

Time discretization included giving an initial time step 1×10^{-4} day, maximum time step 0.1-day, and minimum time step 1×10^{-5} day. The amount of water used for irrigation was added to the rainfall received (Behera and Panda 2011). The daily reference evapotranspiration (ET_0) was calculated using the FAO Penman–Monteith method (Zotarelli et al. 2010). It is used to recognize maximum rates of plant transpiration and soil evaporation. This helps calculate the potential transpiration for the crop (Srivastava et al. 2020).

3.2 Water simulation

The water flow and solute transport in variably saturated porous media in 1D was simulated. The model evaluates the non-steady unsaturated water flow through Richard's equation

$$\frac{\partial \theta}{\partial t} = \frac{\partial}{\partial x}\left[K(h)\left(\frac{\partial h}{\partial x} + \cos\alpha\right)\right] - D \tag{1}$$

where θ is the volumetric soil water content ($cm^3\ cm^{-3}$), h is the water pressure head, and time (days), respectively, x is the spatial coordinate (positive upward), D and α is the sink/drop term ($cm^3\ cm^{-3}\ day^{-1}$) and is the angle between the flow direction, respectively. K is used for unsaturated soil hydraulic conductivity function ($cm\ day^{-1}$). The vertical axis (i.e. $=0°$ for vertical flow, 90° for horizontal flow, and $0° < \alpha < 90°$ for inclined flow. HYDRUS 1D is able to predict the soil moisture data in space and time with satellite data provided for hydro-meteorological modelling applications (Gupta et al. 2014b).

3.2.1 Soil hydraulic model and boundary conditions

Soil water hydraulic properties were the model inputs and calculated using dual-porosity model mobile–immobile water mass transfer for both P and K. The dual-porosity formulation for water flow as used in HYDRUS-1D is based on a mixed formulation, which uses Richards Eq. (1) to describe water flow in the fractures (macropores), and a simple mass balance equation to describe moisture dynamics in the matrix as follows (Šimunek et al. 2003)

$$\frac{\partial \theta_{\mathrm{mo}}}{\partial t} = \frac{\partial}{\partial x}\left[K(h)\left(\frac{\partial h}{\partial x} + \cos\alpha\right)\right] - S_{\mathrm{mo}} - \Gamma_w \tag{2}$$

$$\frac{\partial \theta_{im}}{\partial t} = -S_{\mathrm{im}} - \Gamma_w \tag{3}$$

where, S_{mo} and S_{im} are sink terms for both regions, and Γ_w is the transfer rate for water from the inter- to the intra-aggregate pores.

The built-in Rosetta module in Hydrus 1D calculates hydraulic parameters (Garg and Gupta 2015), which are presented in Table 4. The module gives values of θ_{res} = residual water content, θ_{sat} = saturated water content, p = coefficient related to n, the pore size distribution index (–), n = pore size distribution index (–), k_s = hydraulic conductivity, l = pore connectivity, usually 0.5.

The water flux type of boundary condition was applied at the upper boundary of the soil

$$-K(h)\left(\frac{\partial h}{\partial d} + 1\right)\Big|_{d=0} = s_0(t) \quad \text{for } t > 0 \tag{4}$$

where s_0 ($cm\ day^{-1}$) is the prescribed values of the soil water flux at the upper boundary. A free drainage boundary condition was selected at the bottom of the soil profile,

$$\frac{\partial h}{\partial d} = 0, \quad x = 0 \tag{5}$$

Table 4 Parameters of van Genuchten functions for soil water retention

Treatment	Depth (cm)	θ_r (cm^3 cm^{-3})	θ (cm^3 cm^{-3})	θ (m^{-1})	n	K_s (cm d^{-1})	l
T1	0–5	0.078	0.430	0.036	1.560	24.96	0.5
	5–10	0.073	0.450	0.010	1.509	21.46	0.5
	10–15	0.069	0.424	0.006	1.608	19.52	0.5
	15–30	0.074	0.435	0.007	1.580	17.25	0.5
	30–45	0.068	0.402	0.010	1.5180	09.03	0.5
	45–60	0.063	0.383	0.009	1.524	08.13	0.5
T2	0–5	0.069	0.428	0.011	1.500	15.20	0.5
	5–10	0.070	0.427	0.009	1.536	15.67	0.5
	10–15	0.073	0.433	0.008	1.566	16.03	0.5
	15–30	0.046	0.373	0.008	1.578	26.18	0.5
	30–45	0.057	0.384	0.011	1.502	11.50	0.5
	45–60	0.040	0.344	0.011	1.490	17.48	0.5
T3	0–5	0.052	0.426	0.006	1.627	27.00	0.5
	5–10	0.048	0.435	0.006	1.610	30.02	0.5
	10–15	0.051	0.396	0.006	1.647	18.04	0.5
	15–30	0.067	0.413	0.007	1.584	14.79	0.5
	30–45	0.037	0.350	0.010	1.526	19.00	0.5
	45–60	0.048	0.361	0.010	1.507	12.76	0.5
T4	0–5	0.074	0.453	0.009	1.528	23.86	0.5
	5–10	0.073	0.452	0.010	1.510	22.56	0.5
	10–15	0.070	0.439	0.006	1.617	26.86	0.5
	15–30	0.067	0.413	0.007	1.584	14.79	0.5
	30–45	0.066	0.388	0.010	1.471	16.42	0.5
	45–60	0.061	0.372	0.009	1.496	16.56	0.5

3.3 Solute movement in soil

A dual-porosity model was used for solute transport (Šimunek et al. 2003). The dual-porosity model with physical and chemical non-equilibrium was selected to acknowledge the macropore flow due to the high infiltration rate measured. This model divides fluid flow into mobile and immobile domains with first-order advection and diffusion between the domains. The initial concentration profiles of P and K concentration were measured in the unsaturated soil zone at the start of the study at the time, $t=0$. At the upper soil surface, a concentration boundary condition was applied

$$C(d,t) = c_i(d,0), \quad \text{for } -60 \le d \le 0 \tag{6}$$

where c_i is the initial solute concentration and d = depth of soil profile.

At the lower boundary, a finite column of zero concentration was assumed.

$$\left.\frac{\partial c_i}{\partial d}\right|_{d\to 60} = 0 \tag{7}$$

3.4 Solute transport and reaction parameter

As described above, some of the solute transport parameters required by the numerical model were obtained from the available literature. Longitudinal Dispersion coefficient was taken as 6 cm as conventionally, longitudinal dispersivity has been approximated to be 10% of the sample length in the direction of flow (Lallemand-Barres and Peaudecerf 1978). The calculated infiltration rate was 5.4 cm/h, which justifies the high saturated hydraulic conductivity (K_s) as the field was not puddled. Fraction was taken as 1 as all sorption sites are in contact with mobile water. The saturated volumetric immobile water content was varied from 0.01 (Freiberger et al. 2018) to 1.01. Diffusion coefficient for orthophosphate (most absorbable form of P) in water solution was taken from the average value listed in (Hatfield et al. 1966; Khan et al. 2009). The diffusion coefficient for potassium chloride (Muriate of Potash) was taken from (Lobo et al. 1998; Ernani et al. 2002). K_d (the 'weighted' linear sorption/distribution coefficient) ($cm^3\ mg^{-1}$) for P was adjusted to 14 for loamy soil, which was well within the ranges as compared to earlier studies (Freiberger et al. 2018) and (Qiao 2014) while for K it was taken from (Vilela et al. 2018) for loamy soil. α, solute transfer coefficient was taken from (Freiberger et al. 2018).

3.5 Root water and nutrient uptake

HYDRUS (1D) has a generalized adsorption equation, which may be converted to Freundlich Langmuir or linear adsorption isotherms depending on empirical coefficients. The present study assumed linear adsorption isotherm for P (Freiberger et al. 2018). The value of absorbed P and K was determined by (Feddes et al. 1978) equation as follows, achieved when coefficient $\beta_k = 1$ and $\eta_k = 0$ in Eq. (8)

$$S = \frac{\gamma C^{\beta}}{1 + \eta C^{\beta}} \tag{8}$$

where, S = adsorbed P or K (g/cm^3). γ is the coefficient of root water uptake.

Since pH of the soil shows that the soil was alkaline, saline stress condition selection in the model was ruled out. The solute uptake in water is dependent on Michaelis–Menten constant and the minimum concentration for uptake was taken from Teo et al. (1992), while active root uptake was taken from Teo et al. (1995) for both P and K. The passive root uptake was set at 0.1 for entire crop season as (Qiao 2014).

3.6 Root growth

The root growth parameter in the model is described by the logistic growth function that is defined as follows (Šimunek et al. 2008)

$$D_r(t) = D_m f_r(t) \tag{9}$$

$$f_r(t) = \frac{D_0}{D_o + \left(D_m - D_o\right)e^{-rt}} \tag{10}$$

where, D_r (t) is the root depth at time t (cm); D_o is the initial seeding depth, (cm); D_m is the maximum root depth (cm); t is the number of days after planting; r is the root growth. The maximum root depth of Boro rice was 42 cm.

3.7 Space discretization

The soil profile of 60 cm depth was discretized into 149 linear elements with 150 nodes. Smaller size elements were taken close to the transition zones which were nearer to the surface within the chosen soil depth (Gupta et al. 2012). Galerkin-type linear finite element scheme is used for the spatial distribution of the variables in Eq. (1). All these regions were selected based on their varying soil properties, in order to ensure a real and stable numerical simulation of the model.

4 Performance assessment

Relative root-mean-square error (RMSER), percentage bias (PBIAS), and Nash–Sutcliffe modelling efficiency (E) (Nash and Sutcliffe 1970; Mathevet et al. 2006) are used in assessing the level of agreement between the simulated and measured available P and K concentrations.

RMSER is defined as

$$\text{RMSER} = \frac{\sqrt{MSE}}{\bar{M}} \tag{11}$$

$$MSE = \frac{1}{n}\sum_{i=1}^{n}(M - S)^2 \tag{12}$$

where MSE is the mean square error, $\bar{M}$ is the measured mean value, M is the measured available P or K concentration, S is simulated available P or K concentration corresponding to measured value and n is the number of data points. The smaller the values of RMSER, the better is the match between simulated values and measured values.

Percentage bias (PBIAS) helps in understanding the nature of the simulated data to be smaller or larger from the measured values. The optimal value of PBIAS is 0.00, with low-magnitude values corresponding to more accurate model simulation. Here, positive values correspond to overestimation bias, whereas negative values correspond to model bias underestimation.

$$\text{PBIAS} = 100\frac{\sum_{i=1}^{n}(M - S)}{\sum_{i=1}^{n}M} \tag{13}$$

E is defined as a measure of the deviation of simulated value from measured values.

$$E = 1 - \frac{\sum_{i=1}^{n}(M - S)^2}{\sum_{i=1}^{n}(M - \bar{M})^2} \tag{14}$$

Modelling efficiencies (E) can range from $-\infty$ to 1 where $E=1$ means a perfect match between simulated values and measured data values. A negative E value states that the use

of simulated values can increase the chance of deviation from the measured than using the mean observation. $E=0$ indicates that the model predictions are as close as the mean of the measured data.

5 Results and discussion

5.1 Evaluation of soil and crop data

The soil of the site has been classified as alluvial soil. Soil physical properties were analysed (Table 5) for the soil profile of 0–60 cm at an interval mentioned above with three replicates. The percentages of sand, silt, and clay were determined by Bouyoucos Hydrometer. The texture percentage was utilized in the determination of soil type based on the soil textural triangle (USDA). The soil type was found to be loamy in all the plots with a slight variation at 10–30 cm depth for Plot 3 and 4, where the soil was silty loam. Bulk density was estimated from the soil samples on the field. The soil organic matter (SOM) was calculated using the method given by (Walkley and Black 1934). The Keen Rackzowski box (Keen and Raczkowski 1921; Salalia and Walia 2017) was used to calculate the field capacity. Eutechmeter was used to measure soil pH and Electrical Conductivity (EC).

The meteorological data for the study period are shown in Fig. 3. The data for crop growth (LAI) and root growth were also collected from the field at regular intervals, which are used as input in HYDRUS 1D. These parameters are shown in Fig. 4. Figure 5 shows the image of photographs taken on 34 days after application of entire plants for each of the four treatments.

5.2 Model parameterization and establishment

The values of various coefficients taken from the literature were varied according to the soil conditions and climate. Some of the coefficients were found to be more sensitive than the others. The sensitivity analysis was done to check with minimal change in input parameters there was a maximal change in output parameters. The ranges of dual-porosity coefficients were taken from Haws et al. (2005) and were then varied one at a time to see the most sensitive parameter. The combination of varying these variables was also done within

Table 5 Soil physical properties

Depth (cm)	Soil pH	EC	%Sand	% Silt	%Clay	Soil type[a]	Bulk density (g/cm^3)	Avg. %SOM	Field capacity (%)
0–5	7.79	86.74	41.88	19.86	38.25	Loamy	1.27	0.797	23.22
5–10	7.79	86.10	41.92	19.43	38.65	Loamy	1.27	0.865	22.92
10–15	7.87	78.10	35.58	16.86	46.65	Loamy	1.32	1.014	22.45
15–30	7.79	80.46	36.84	15.75	47.40	Loamy	1.45	1.190	21.20
30–45	8.10	65.12	38.44	16.55	45.00	Loamy	1.50	0.784	19.76
45–60	7.91	64.55	39.50	18.35	42.15	Loamy	1.50	0.703	19.60

[a]Average texture for all plots is considered as loamy

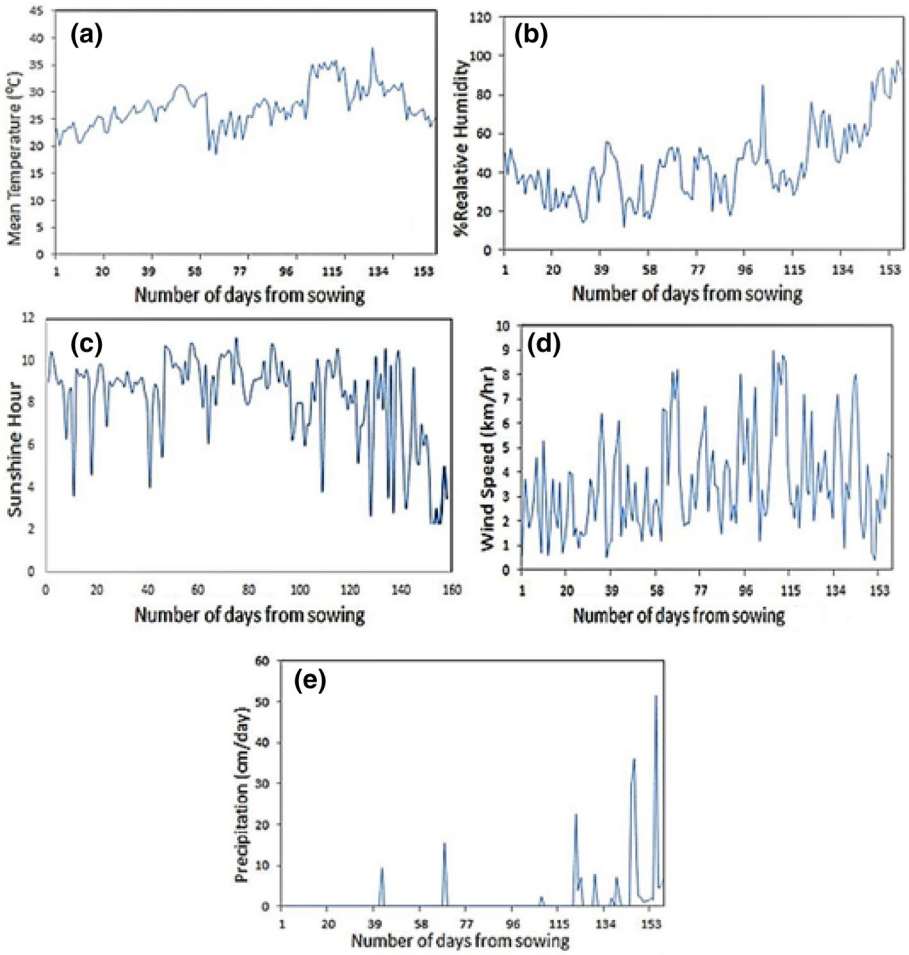

Fig. 3 Meteorological parameters used in the study

the range found in the literature. The root active uptake was found to be the most sensitive and after much calibration was set at 0.01. The solute uptake in water is dependent on Michaelis–Menten constant and minimum concentration for uptake which was varied between 0.5 to 0.0062 and 0.1 to 0.0023, respectively (Yan Hock Teo et al. 1995). The partition coefficient (Sikder and Hossain 2018) was varied between 6 to 17 for available P and 5 to 8 for K. The immobile water concentration was varied between 0.01 and 1.01 and the selected range was 0.05–1.01. The irrigation water was also having P whose value was taken in g/m^3 from groundwater yearbook 2014–2015 (Uttar Pradesh), and then values were adjusted according to irrigation water volume. The coefficient calibration was carried out for T1 only. After calibrating these parameters for T1, the average simulated concentration along with the measured concentration for calibration treatment is shown in Fig. 6a, b for K and available P, respectively. The statistical measures for the same are also presented in Table 6. The average E achieved during calibration in the soil profile was 0.54 and 0.47 for available P and K respectively. The validation was performed for T2, T3, and T4 using

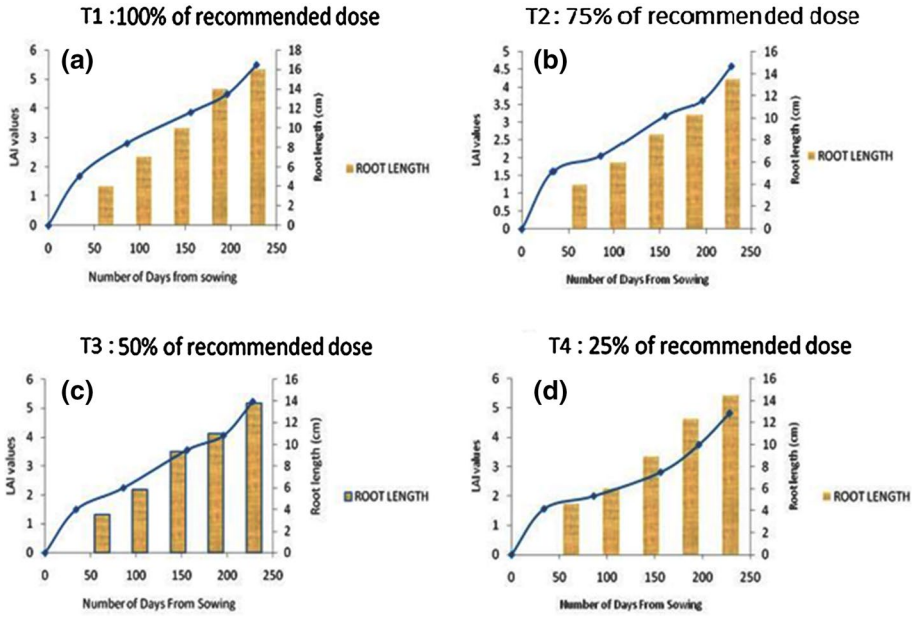

Fig. 4 Root length measurement record for entire crop growth period **a** 100%, **b** 75%, **c** 50%, **d** 25% of recommended fertilizer dose

Fig. 5 Root length **a** 100%, **b** 75%, **c** 50%, **d** 25% of recommended fertilizer dose after 34 DAA

the calibrated parameters. Here, all the coefficient values were kept the same as in T1, and data like fertilizer's concentration, the volume of water added, root length, LAI, bulk density, soil hydraulic parameters, and initial concentration of P were changed as measured on the field for the three treatments – T2, T3, T4. The average simulated concentration along with the measured concentration for validation treatments are shown in Fig. 6c, d for K and available P, respectively. Overall plot analysis in Fig. 6c, d for K and available P shows that the simulated data follow the measured data trend for T2 and T3 in the soil profile.

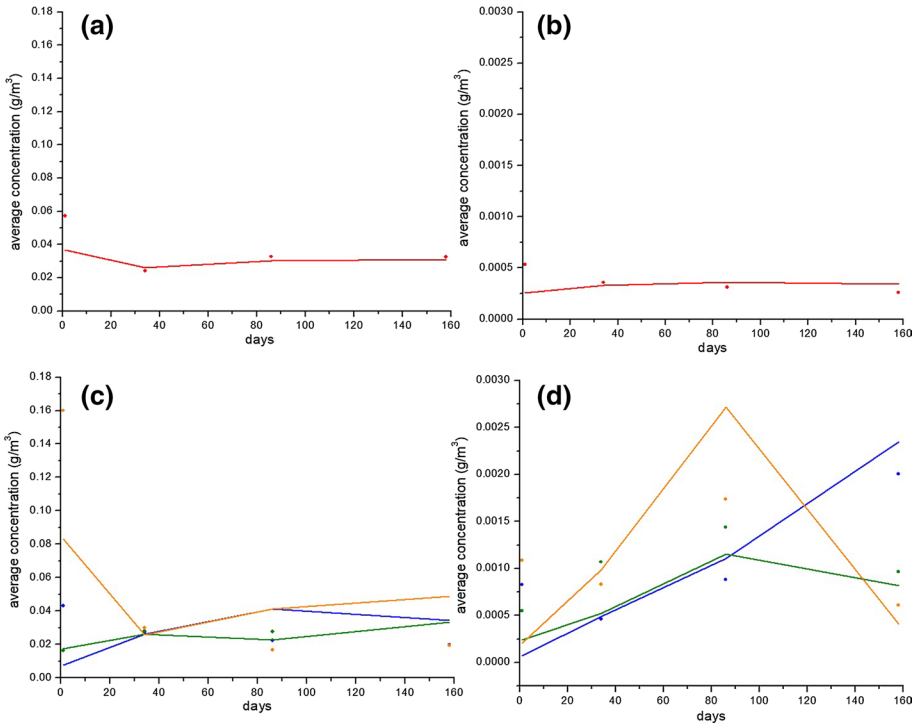

Fig. 6 Average concentration simulated and measured: (a) Potassium: (red solid line, red circle) T1, (b) Phosphorus: (red solid line, red circle) T1, (c) Potassium: (blue solid line, blue circle) T2, (green solid line, green circle) T3, (yellow solid line, yellow circle) T4 and (d) Phosphorus: (blue solid line, blue circle) T2, (green solid line, green circle) T3, (yellow solid line, yellow circle) T4

Simulated concentration values were then also statistically compared with measured values, shown in Table 6, to quantify the agreement for the validation scenario. As given in Table 6, the efficiency agreement within depths and treatments went up to 0.94. However, the average E in the soil profile of 60 cm depth for the three treatments, T2, T3, and T4 is 0.23, 0.50, and 0.89, respectively, for available P and 0.30, 0.57 and 0.80, respectively, for K. The validation results suggest that HYDRUS 1D can be utilized for available P and K simulations with proper calibration.

5.3 Performance of model with different depths and treatments

The treatments in each plot depend upon the variation of concentration of K and available P from the recommended dose. Figures 7a and 8a show the depth-wise variation in concentration from the recommended dose of fertilizer in T1 for K and P, respectively, under Boro rice cultivation obtained after the calibration of the input parameters. Although the modelled values for both the elements are little overestimated, the model shows the closest agreement on 34 days after application (DAA) for both which is shown in Table 6, i.e. with RMSER and E values of 0.445 and 0.806 for potassium and 0.496 and 0.728 for P, respectively. The lowest P concentration was recorded for the T1 among all the other treatments

Table 6 Statistical performance analysis for K and P concentrations

Operations	Treatments	Days	Statistical analysis for K			Statistical analysis for P		
			RMSER	PBIAS	E	RMSER	PBIAS	E
Calibration	T1	1	0.738	35.841	0.435	1.370	51.801	0.040
		34	0.445	− 7.786	0.806	0.496	07.309	0.728
		86	1.040	23.591	0.352	0.522	− 15.910	0.759
		158	0.685	− 42.710	0.412	0.746	− 32.536	0.634
Validation	T2	1	1.014	94.522	0.032	1.144	0.916	0.067
		34	0.433	4.626	0.774	0.877	− 0.143	0.551
		86	1.862	− 85.296	0.324	0.905	− 0.072	0.082
		158	0.861	− 74.437	0.096	0.897	21.741	0.447
	T3	1	0.278	− 6.606	0.910	1.035	0.341	0.052
		34	0.470	7.486	0.747	0.796	0.839	0.770
		86	0.907	17.745	0.300	0.615	1.119	0.686
		158	0.797	− 73.395	0.328	0.501	− 0.530	0.262
	T4	1	0.459	30.376	0.857	0.232	3.990	0.938
		34	0.536	13.266	0.602	0.388	− 0.638	0.802
		86	0.728	− 14.689	0.716	0.452	− 0.210	0.941
		158	0.884	− 15.115	0.956	0.468	− 0.766	0.904

as the plant growth was the highest in this treatment; hence, it consumed the most available P available to it.

Figures 7b and 8b represent T2 for K and available P concentration, respectively. The graph suggests that mostly the model underestimated concentration. The model efficiency was found to be lowest at depths 30–60 cm for both the elements. This shows the model's inability to predict the concentration at later days and deeper depths of the crop. The measured concentration at (0–10) cm at 1DAA in the case of K and (5–15) cm at 158 DAA in the case of available P was considered as an outlier from the pattern as shown in Figs. 7b and 8b. This uneven concentration can easily be pointed out with the underestimated results of PBIAS. The PBIAS clearly shows more than underestimation at all DAA by the model unlike the simulated values of T1 treatment plots for both the elements. The *E* value varies from 0.032 to 0.774 for K and 0.067 to 0.551 for available P (Table 6). The RMSER suggests that the model simulated values are most appropriate at 34 DAA. Figures 7c and 8c depict depth-wise variation for T3 for simulated K and available P concentration values, respectively. The model simulated values are more in agreement with real values at all depths almost at all DAA of fertilizer for both the element P and K. The PBIAS values suggest that the model simulated concentrations, in general, are underestimated (Table 6).

Similarly, Figs. 7d and 8d represent a depth-wise variation of T4 for K and available P concentration, respectively. These two figures highlight the best agreement at all DAA at all depths. The E values for T4, Table 6, were found consistently high among other treatments, suggesting good agreement between the measured and simulated concentrations for both K and P. The RMSER and PBIAS values were also lowest for T4 ranging from 0.232 to 0.884 and − 0.210 to 30.376. PBIAS values suggest little overestimation in the case of P.

The day-wise variations in Figs. 9 and 10 for K and available P for all treatments, showed that model values are in close range with the measured values at all days and depth except at the depth between (30 and 60) cm at 86 and 158 DAA. Either the model

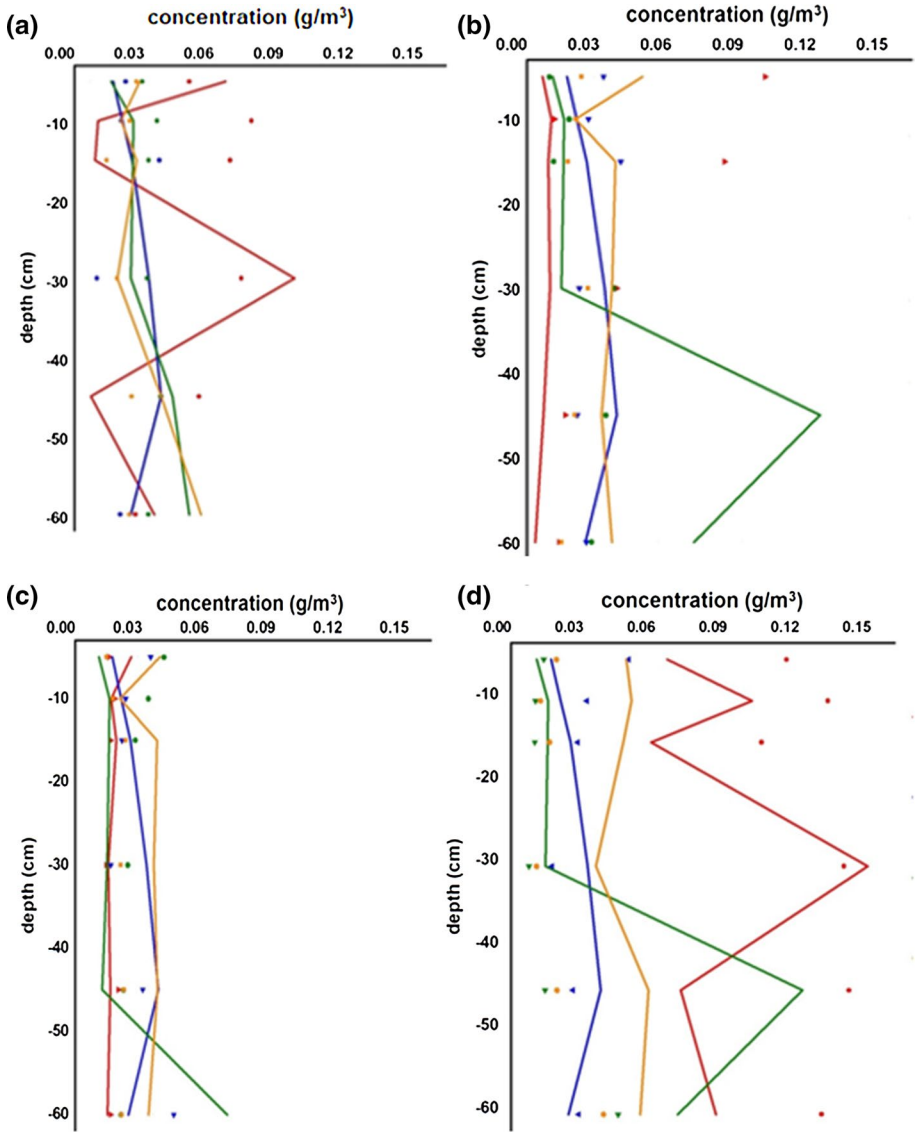

Fig. 7 Potassium simulated and measured concentration within 60 cm at (red solid line, red circle) 0 DAA, (blue solid line, blue inverted triangle) 34 DAA, (green solid line, green right triangle) 86 DAA, (yellow solid line, yellow circle) 156 DAA for treatments **a** T1, **b** T2, **c** T3 and **d** T4, respectively

simulation underestimates or overestimates at these depths and days. The least efficiency is encountered in simulating at 0–5 cm and 30–60 cm for either of the element simulated. Statistical performance for measured K concentration at the end of 158 DAA was less accurate than that of the available P at the end of 158 DAA although both the element's concentration was easily traceable in the soil at the end of crop period. This suggests the model is more suitable for simulation of available P than K at lower concentration levels.

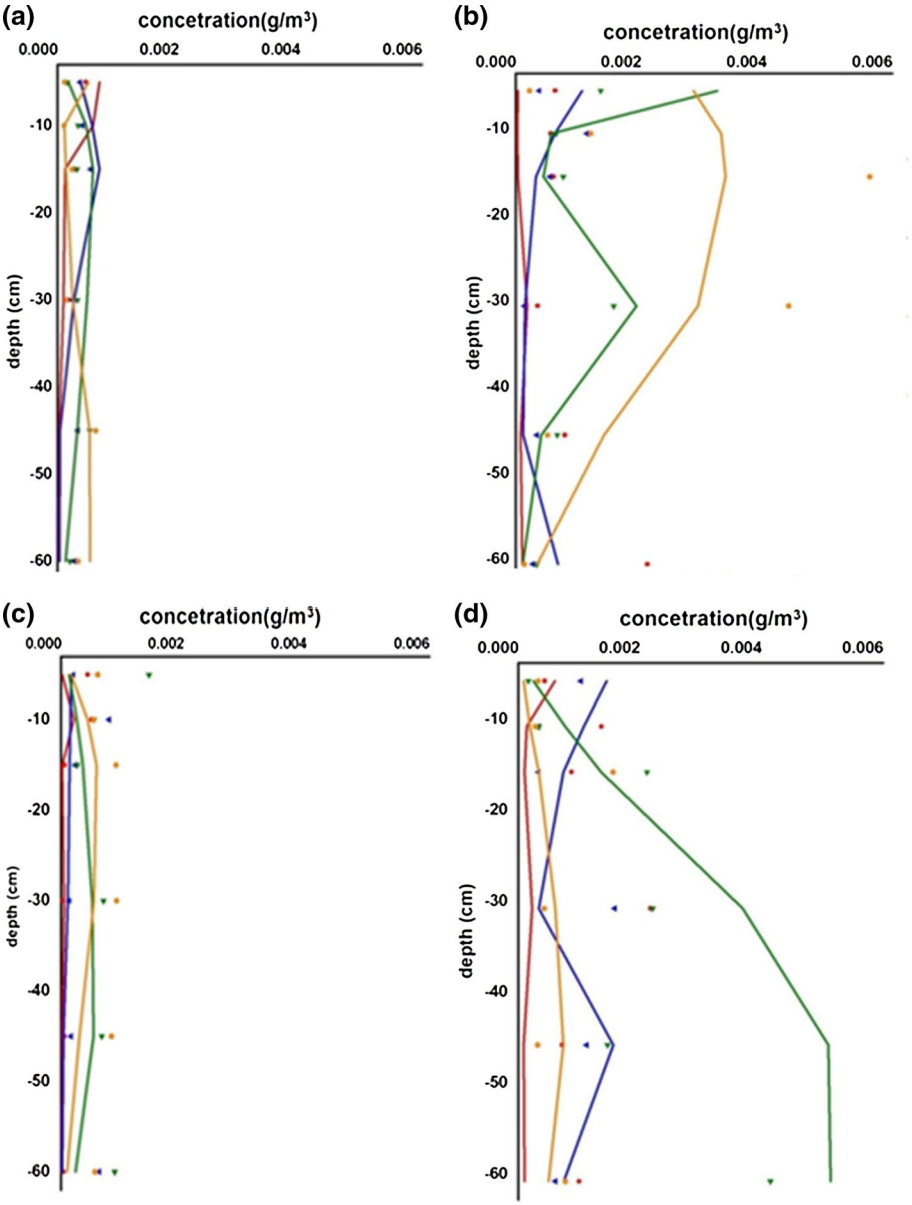

Fig. 8 Phosphorous simulated and measured concentration within 60 cm at (red solid line, red circle) 0 DAA, (blue solid line, blue inverted triangle) 34 DAA, (green solid line, green right triangle) 86 DAA, (yellow solid line, yellow circle) 156 DAA for treatments **a** T1, **b** T2, **c** T3 and **d** T4, respectively

In this experiment after analysing every treatment chosen, it can be seen that the simulated values at mid days of the crop are closer to measured values than later days, 158 DAA of fertilizer where it mostly underestimates. This may be due to the fact that currently, the selection of crops in the HYDRS 1D version is very limited. The closest crop relating to

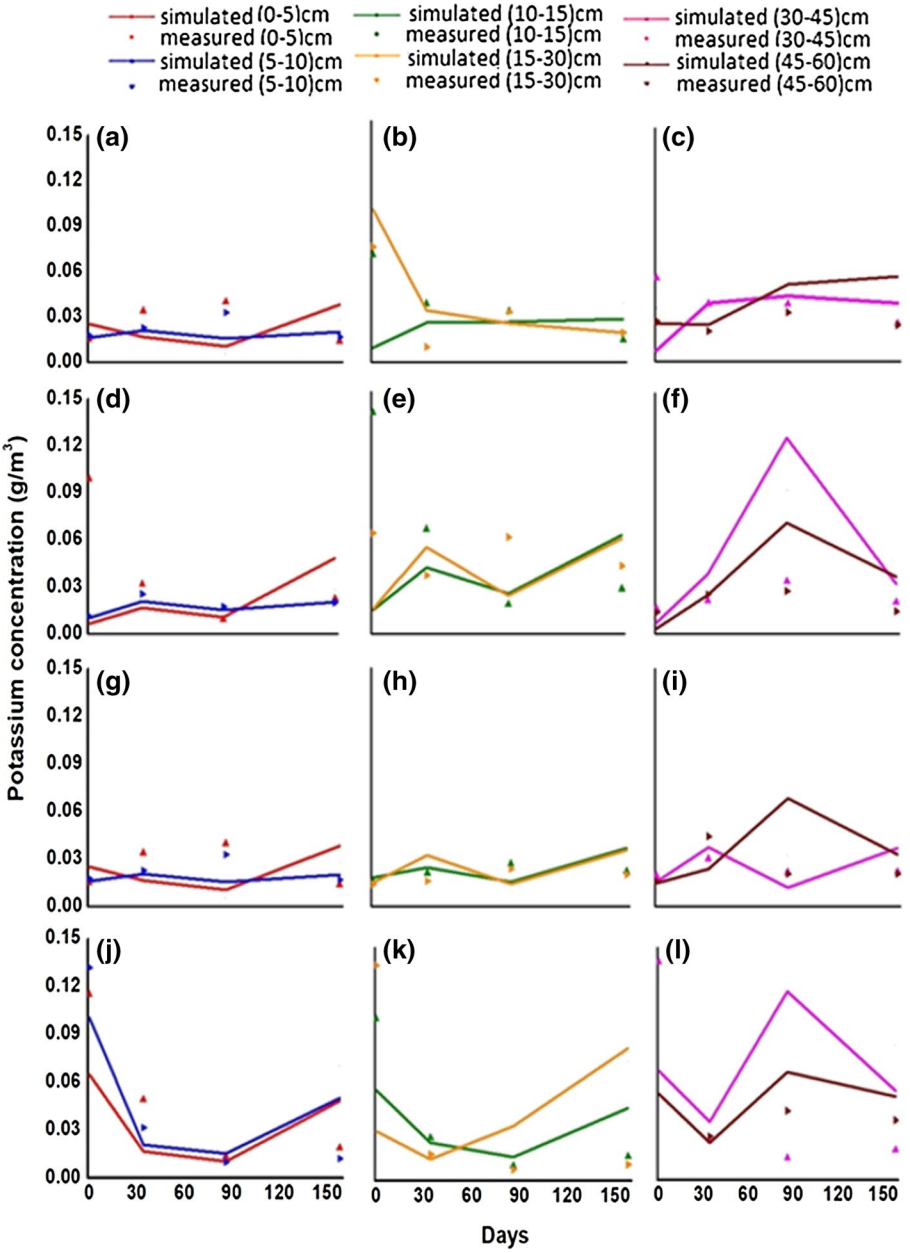

Fig. 9 Potassium at depths as per legends: **a**–**c** (T1), **d**–**f** (T2), **g**–**i** (T3), and **j**–**l** (T4)

Boro rice found was corn crop but even the corn crop duration is 180 days. This may be the reason of the constant underestimation from the real values at later days of the crop. The model shows best results with T4 (25%—from the recommended dose) with the calibrated values as compared to T2 and T3. The reduction in the concentration of fertilizer reduces

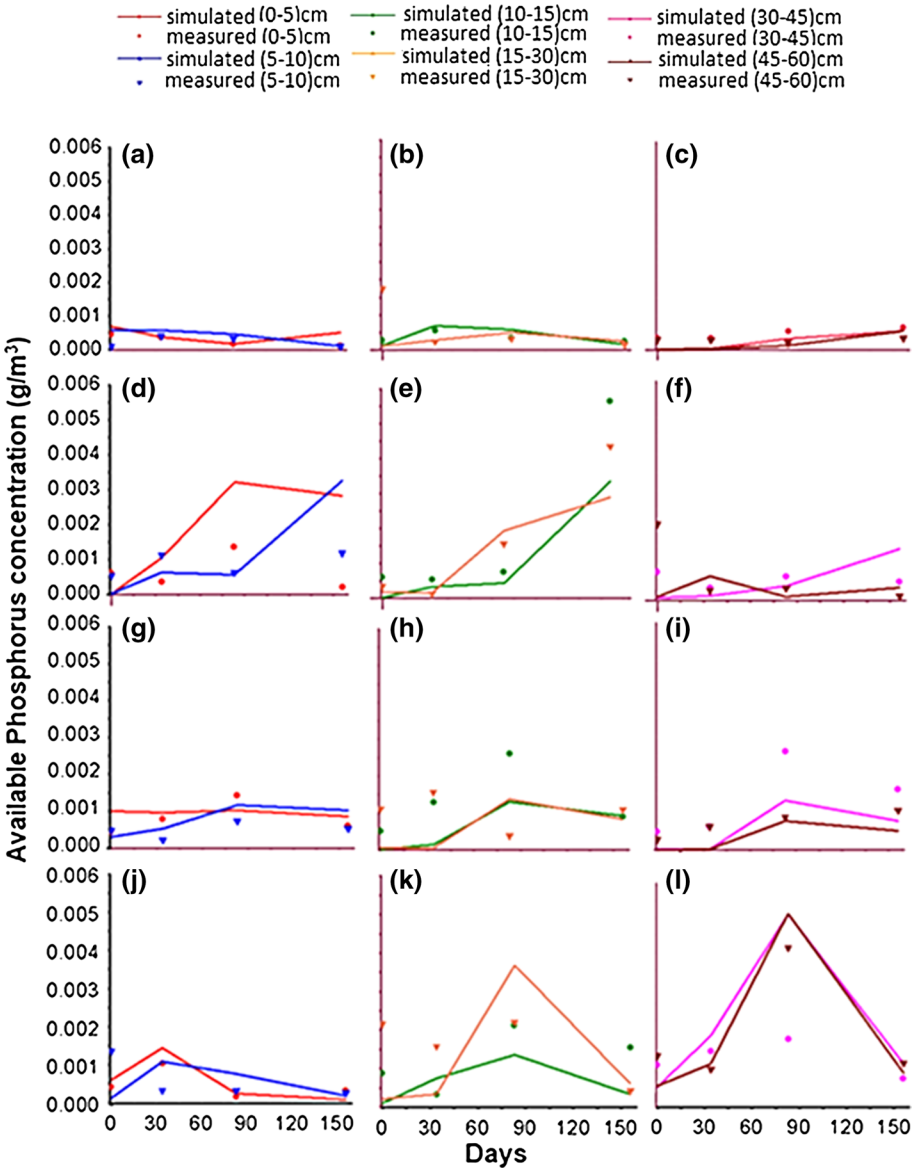

Fig. 10 Available P at depths as per legends: **a–c** (T1), **d–f** (T2), **g–i** (T3), and **j–l** (T4)

the difference between the measured and real values. Hence, low concentration is found to be simulated efficiently by the model. Since the direct-seeded rice crops are not covered in the HYDRUS 1D model, other versions like HYDRUS NICA (Non-Ideal Competitive Adsorption) with an aqueous chemical model NICA might be more suitable for elements like P to improve the simulations of P transport in soil and water (Nohra et al. 2004).

The constant high measured values of available P in the field samples at later stages of the crop cycle may be attributed to nitrogen fertilizer added in splits. Nitrogen

fertilizer releases NH_4^+ ions, which makes the soil acidic and in turn increases P solubilization. P solubilization leads to an increase in P availability. Nitrogen in the soil also results in a surge of P uptake by increasing plant root length and P availability in soil (Havlin et al. 2016). Exchangeable K ions (40–500 ppm) hold on to the solid phase of soil on clay and organic matter by electrostatic forces and moves into the soil solution through exchange with other cations. In soil solution where hydrated Ca^{2+} is bigger than K, it enlarges the interspace layer which is compensated by more K^+ (Sekhon 1999). Since at deeper depths (45–60) cm clay content was more (Table 5) and at later days of the crop (86 DAA) highest organic matter content was also measured, which explains the increase in K at later days of the crop (i.e. either 86 DAA or 158 DAA).

The cation complex may also have increased in later DAA of fertilizer due to direct sowing of seed without ploughing (while preparing the seedbed). Additionally, the field was prepared without puddling and that may have also contributed to high organic matter and hence the increase in K concentration (Benedetti et al. 1996; Haefele et al. 2011). The K and P concentration at deeper depths (45–60) cm) layer of soil is dynamic and is constantly high in concentration than the rest of the other layers due to the absence of roots or less availability of roots to extract these minerals.

6 Conclusion

In this study, four Boro rice crop plots were chosen with variations in the amount of K, available P from the recommended dose of fertilizer. The behaviour, tenacity, and movement of K and available P were studied by determining the concentration of K and P in soil experimentally and numerically using the HYDRUS 1D model. The model was found suitable for simulating K and available P concentration in soil with Boro rice crop after careful calibration of parameters. The comparison between the simulated and observed data suggests that the model is more suitable for simulations at low-level concentrations of K and P than higher concentration levels. This analysis also makes it evident that the model is more suitable for upper depths up to 45 cm than the lower depths (45–60 cm). Also, the model predicted well in early days of the crop rather than in later days.

The study also indicates regulation in fertilizer application can be brought using the HYDRUS 1D model. The numerical simulations with the recommended fertilizer dose can help in predicting the residual K and available P in the soil at the end of the crop cycle as in the current study traceable amounts were detected after 158 DAA. Although their transformation and degradation can occur reducing the residue of the elements in soil, two cropping seasons in India may likely lead to persistence rather than being degradation. Thus, simulations can help in regulating fertilizer dose reducing carry-over effects, which may ultimately lead to the safer dosage and better management of K and P applications in soil. Sustainability in agriculture can only be brought by regulating traditional agriculture practices by accounting for these non-point anthropogenic sources.

Acknowledgements The authors thank the University Grant Commission for financial support. Authors are also thankful for SAP funding provided by UGC to the Department of Agronomy, Institute of Agricultural Sciences, Banaras Hindu University. The authors also acknowledge Institute of Environment and Sustainable Development, Banaras Hindu University for providing the necessary laboratory support for the study.

Compliance with ethical standards

Conflict of interest None.

References

Behera, S., & Panda, R. (2011). Assessing soil and groundwater contamination with HYDRUS-1D: A study from West Bengal. *Environmental Quality Management, 20*(3), 59–75.

Benedetti, M. F., Van Riemsdijk, W. H., Koopal, L. K., Kinniburgh, D. G., Gooddy, D. C., & Milne, C. J. (1996). Metal ion binding by natural organic matter: from the model to the field. *Geochimica et Cosmochimica Acta, 60*(14), 2503–2513.

CO, A., et al. (2011). Rice production and water use efficiency for self-sufficiency in Malaysia: A review. *Trends in Applied Sciences Research, 6*(10), 1127–1140.

De Datta, S. (1986). Improving nitrogen fertilizer efficiency in lowland rice in tropical Asia. In *Nitrogen economy of flooded rice soils* (pp. 171–186). Berlin: Springer.

Ernani, P. R., Dias, J., & Flore, J. A. (2002). Annual additions of potassium to the soil increased apple yield in Brazil. *Communications in Soil Science and Plant Analysis, 33*(7–8), 1291–1304.

Feddes, R., Kowalik, P., & Zaradny, H. (1978). *Simulation of field water use and crop yield. Simulation monographs* (pp. 9–30). Wageningen: Pudoc.

Freiberger, R. P., Heeren, D. M., Eisenhauer, D. E., Mittelstet, A. R., & Baigorria, G. (2018). Tradeoffs in model performance and effort for long-term phosphorus leaching based on in situ field data. *Vadose Zone Journal, 17*(1), 1–12.

Garg, N., & Gupta, M. J. I. S. (2015). Assessment of improved soil hydraulic parameters for soil water content simulation and irrigation scheduling. *Irrigation Science, 33*(4), 247–264.

Gupta, M., Garg, N., Joshi, H., & Sharma, M. (2012). Persistence and mobility of 2, 4-D in unsaturated soil zone under winter wheat crop in sub-tropical region of India. *Agriculture, Ecosystems & Environment, 146*(1), 60–72.

Gupta, M., Garg, N., Joshi, H., Sharma, M. J. E., et al. (2014a). Assessing the impact of irrigation treatments on thiram residual trends: Correspondence with numerical modelling and field-scale experiments. *Environmental Monitoring and Assessment, 186*(3), 1639–1654.

Gupta, M., Srivastava, P. K., Islam, T., & Ishak, A. M. B. J. E. E. S. (2014b). Evaluation of TRMM rainfall for soil moisture prediction in a subtropical climate. *Environmental Earth Sciences, 71*(10), 4421–4431.

Haefele, S., Konboon, Y., Wongboon, W., Amarante, S., Maarifat, A., Pfeiffer, E., et al. (2011). Effects and fate of biochar from rice residues in rice-based systems. *Field Crops Research, 121*(3), 430–440.

Hatfield, J., Edwards, O., & Dunn, R. (1966). Diffusion coefficients of aqueous solutions of ammonium and potassium orthophosphates at 25°. *The Journal of Physical Chemistry, 70*(8), 2555–2561.

Havlin, J. L., Tisdale, S. L., Nelson, W. L., & Beaton, J. D. (2016). *Soil fertility and fertilizers*. Chennai: Pearson Education India.

Haws, N. W., Rao, P. S. C., Simunek, J., & Poyer, I. C. (2005). Single-porosity and dual-porosity modeling of water flow and solute transport in subsurface-drained fields using effective field-scale parameters. *Journal of Hydrology, 313*(3–4), 257–273.

INTER, I. (2011). Toolkit for identification and quantification of mercury releases.

Keen, B. A., & Raczkowski, H. (1921). The relation between the clay content and certain physical properties of a soil. *The Journal of Agricultural Science, 11*(4), 441–449.

Khan, A. A., Jilani, G., Akhtar, M. S., Naqvi, S. M. S., & Rasheed, M. (2009). Phosphorus solubilizing bacteria: Occurrence, mechanisms and their role in crop production. *J agric biol sci, 1*(1), 48–58.

Lal, B., Gautam, P., Panda, B., & Raja, R. (2013). Boro rice: a way to crop intensification in Eastern India.

Lallemand-Barres, A., & Peaudecerf, P. (1978). Investigation of the relationship between the value of the macroscopic dispersiveness of an aquifer medium, its other characteristics, and the measurement conditions—Bibliographic study. *Bull BRGM Ser, 2*(3), 4.

Lobo, V. M., Ribeiro, A. C., & Verissimo, L. M. (1998). Diffusion coefficients in aqueous solutions of potassium chloride at high and low concentrations. *Journal of Molecular Liquids, 78*(1–2), 139–149.

Masto, E. (2004). Soil quality assessment in maize-wheat-cowpea cropping system under long-term fertiliser USE. Division of Soil Science And Agricultural Chemistry Indian Agricultural.

Mathevet, T., Michel, C., Andreassian, V., & Perrin, C. (2006). A bounded version of the Nash-Sutcliffe criterion for better model assessment on large sets of basins. *IAHS Publication, 307,* 211.

Moterle, D. F., Kaminski, J., dos Santos Rheinheimer, D., Caner, L., & Bortoluzzi, E. C. (2016). Impact of potassium fertilization and potassium uptake by plants on soil clay mineral assemblage in South Brazil. *Plant and Soil, 406*(1–2), 157–172.

Nash, J. E., & Sutcliffe, J. V. (1970). River flow forecasting through conceptual models part I—A discussion of principles. *Journal of Hydrology, 10*(3), 282–290.

Nohra, J. A., Madramootoo, C., & Hendershot, W. (2004). Modeling phosphorus transport in soil and water. In *2004 ASAE annual meeting*. American Society of Agricultural and Biological Engineers (p. 1).

Pawar, D., Shah, K. J. G. O. M. W. R. D., Directorate of Irrigation Research, & Development, P. (2009). Laboratory testing procedure for soil and water sample analysis.

Qiao, S. Y. (2014). *Modeling water flow and phosphorus fate and transport in a tile-drained clay loam soil using HYDRUS (2D/3D)*. Montreal: McGill University Libraries.

Salalia, R., & Walia, R. (2017). Effect of soil texture and water regimes on the pathogenicity of rice root-knot nematode, meloidogyne graminicola on rice. *Indian Journal of Nematology, 47*(1), 136–138.

Sarangi, S. K., Maji, B., Singh, S., Sharma, D. K., Burman, D., Mandal, S., et al. (2014). Crop establishment and nutrient management for dry season (boro) rice in coastal areas. *Agronomy Journal, 106*(6), 2013–2023.

Sekhon, G. (1999). Potassium in Indian soils and crops. *Proceedings of Indian National Science Academy B, 65,* 83–108.

Sikder, M. S., & Hossain, F. (2018). Improving operational flood forecasting in monsoon climates with bias-corrected quantitative forecasting of precipitation. *International Journal of River Basin Management, 17,* 1–11.

Šimůnek, J., Jarvis, N. J., Van Genuchten, M. T., & Gärdenäs, A. (2003). Review and comparison of models for describing non-equilibrium and preferential flow and transport in the vadose zone. *Journal of Hydrology, 272*(1–4), 14–35.

Šimůnek, J., & van Genuchten, M. T. (2008). Modeling nonequilibrium flow and transport processes using HYDRUS. *Vadose Zone Journal, 7*(2), 782–797.

Šimůnek, J., van Genuchten, M. T., & Šejna, M. (2008). Development and applications of the HYDRUS and STANMOD software packages and related codes. *Vadose Zone Journal, 7*(2), 587–600.

Singh, R. (2003). Harnessing Boro rice potential for increasing rice production in deepwater areas of eastern India: an overview. *Boro Rice*.

Srivastava, P. K., Singh, P., Mall, R., Pradhan, R. K., Bray, M., Gupta, A. J. T., et al. (2020). Performance assessment of evapotranspiration estimated from different data sources over agricultural landscape in Northern India, 1–12.

Teo, Y., Beyrouty, C., & Gbur, E. (1992). Nitrogen, phosphorus, and potassium influx kinetic parameters of three rice cultivars. *Journal of Plant Nutrition, 15*(4), 435–444.

Teo, Y. H., Beyrouty, C. A., Norman, R. J., & Gbur, E. E. (1995). Nutrient uptake relationship to root characteristics of rice. *Plant and Soil, 171*(2), 297–302.

Vilela, N., Thebaldi, M. S., Leal, B. D. P., Silva, A. V., & Martins, I. P. (2018). Transport parameters of potassium from different sources in soil columns. *Engenharia Agrícola, 38*(1), 135–141.

Walkley, A., & Black, I. A. (1934). An examination of the Degtjareff method for determining soil organic matter, and a proposed modification of the chromic acid titration method. *Soil Science, 37*(1), 29–38.

Zotarelli, L., Dukes, M. D., Romero, C. C., Migliaccio, K. W., & Morgan, K. T. (2010). *Step by step calculation of the Penman–Monteith evapotranspiration (FAO-56 method)*. Florida: Institute of Food and Agricultural Sciences, University of Florida.

Terms and Conditions

Springer Nature journal content, brought to you courtesy of Springer Nature Customer Service Center GmbH ("Springer Nature").

Springer Nature supports a reasonable amount of sharing of research papers by authors, subscribers and authorised users ("Users"), for small-scale personal, non-commercial use provided that all copyright, trade and service marks and other proprietary notices are maintained. By accessing, sharing, receiving or otherwise using the Springer Nature journal content you agree to these terms of use ("Terms"). For these purposes, Springer Nature considers academic use (by researchers and students) to be non-commercial.

These Terms are supplementary and will apply in addition to any applicable website terms and conditions, a relevant site licence or a personal subscription. These Terms will prevail over any conflict or ambiguity with regards to the relevant terms, a site licence or a personal subscription (to the extent of the conflict or ambiguity only). For Creative Commons-licensed articles, the terms of the Creative Commons license used will apply.

We collect and use personal data to provide access to the Springer Nature journal content. We may also use these personal data internally within ResearchGate and Springer Nature and as agreed share it, in an anonymised way, for purposes of tracking, analysis and reporting. We will not otherwise disclose your personal data outside the ResearchGate or the Springer Nature group of companies unless we have your permission as detailed in the Privacy Policy.

While Users may use the Springer Nature journal content for small scale, personal non-commercial use, it is important to note that Users may not:

1. use such content for the purpose of providing other users with access on a regular or large scale basis or as a means to circumvent access control;
2. use such content where to do so would be considered a criminal or statutory offence in any jurisdiction, or gives rise to civil liability, or is otherwise unlawful;
3. falsely or misleadingly imply or suggest endorsement, approval , sponsorship, or association unless explicitly agreed to by Springer Nature in writing;
4. use bots or other automated methods to access the content or redirect messages
5. override any security feature or exclusionary protocol; or
6. share the content in order to create substitute for Springer Nature products or services or a systematic database of Springer Nature journal content.

In line with the restriction against commercial use, Springer Nature does not permit the creation of a product or service that creates revenue, royalties, rent or income from our content or its inclusion as part of a paid for service or for other commercial gain. Springer Nature journal content cannot be used for inter-library loans and librarians may not upload Springer Nature journal content on a large scale into their, or any other, institutional repository.

These terms of use are reviewed regularly and may be amended at any time. Springer Nature is not obligated to publish any information or content on this website and may remove it or features or functionality at our sole discretion, at any time with or without notice. Springer Nature may revoke this licence to you at any time and remove access to any copies of the Springer Nature journal content which have been saved.

To the fullest extent permitted by law, Springer Nature makes no warranties, representations or guarantees to Users, either express or implied with respect to the Springer nature journal content and all parties disclaim and waive any implied warranties or warranties imposed by law, including merchantability or fitness for any particular purpose.

Please note that these rights do not automatically extend to content, data or other material published by Springer Nature that may be licensed from third parties.

If you would like to use or distribute our Springer Nature journal content to a wider audience or on a regular basis or in any other manner not expressly permitted by these Terms, please contact Springer Nature at

onlineservice@springernature.com